The Tropical Precipitation Response to Andes Topography and Ocean Heat Fluxes in an Aquaplanet Model

ELIZABETH A. MAROON, DARGAN M. W. FRIERSON, AND DAVID S. BATTISTI

Department of Atmospheric Sciences, University of Washington, Seattle, Washington

(Manuscript received 8 March 2014, in final form 8 September 2014)

ABSTRACT

This aquaplanet modeling study using the Geophysical Fluid Dynamics Laboratory Atmospheric Model, version 2.1 (GFDL AM2.1), examines how ocean energy transport and topography influence the location of tropical precipitation. Adding realistic Andes topography regionally displaces tropical rainfall from the equator into the Northern Hemisphere, even when the wind–evaporation feedback is disabled. The relative importance of the Andes compared to the asymmetric hemispheric heating of the atmosphere by ocean transport is examined by including idealized and realistic zonally averaged surface heat fluxes (also known as q fluxes) in the slab ocean. A hemispherically asymmetric q flux displaces the tropical rainfall toward the hemisphere receiving the greatest heating by the ocean. The zonal-mean displacement of rainfall is greater in simulations with a realistic q flux than with a realistic Andes topography. Simulations that add both a q flux and topography displace rainfall farther to the north in the region 120° to the west of the Andes than in simulations that only have a q flux. Cloud and clear-sky radiative feedbacks in the tropics and subtropics of this model both act to amplify the energy flux and the precipitation response to a given hemispheric asymmetry in oceanic forcing.

1. Introduction

More precipitation falls in the Northern Hemisphere (NH) tropics than in the Southern Hemisphere (SH) tropics annually. The zonally averaged tropical precipitation is tied to the ascending branch of the Hadley circulation, also known as the intertropical convergence zone (ITCZ) (Hadley 1735; Dima and Wallace 2003). However, the variation of precipitation from the zonal mean is more complex. Tropical rain over land follows the seasonal cycle of insolation, but the precipitation patterns over the world's oceans differ from basin to basin (Mitchell and Wallace 1992; Waliser and Gautier 1993; Schumacher and Houze 2003). For the majority of the year, there is greater precipitation in the NH of the Atlantic and Pacific Ocean basins, while there is greater precipitation in the SH of the Indian Ocean (Adler et al. 2003; Huffman et al. 2007). Only during the months of March and April is there an equivalent or greater amount of rain in the SH of the Pacific basin. Sometimes there is a double ITCZ, a feature that current general circulation models (GCMs) struggle to capture accurately (Mechoso et al. 1995; Zhang 2001; Hwang and Frierson 2013).

This greater NH precipitation has often been explained through processes and mechanisms local to the tropics. Philander et al. (1996) suggest that the NH Pacific and Atlantic ITCZ is a result of tropical coastal configuration preferring cold water coastal upwelling in the eastern side of the basin, south of the equator. This cold water, in turn, drives a wind–evaporation–sea surface temperature (WES) feedback that further pushes more precipitation to the NH tropics (Xie and Philander 1994). If waters are colder in the SH, then a cross-equatorial pressure gradient is induced that drives a southerly wind across the equator. In the SH, the anomalous higher pressure results in anticyclonic motion that enhances the trade winds to the south of the equator, and in the NH, anomalous lower pressure results in cyclonic motion that decreases trade winds near the equator. Just south of the equator, the stronger trade winds enhance evaporation, which further cools the surface near the equator in the SH, and the opposite occurs in the NH. Thus, changes in the trade winds on both sides of the equator reinforce the changes in SST. Southerly winds across the equator advect moisture to

Corresponding author address: Elizabeth A. Maroon, Department of Atmospheric Sciences, University of Washington, P.O. Box 351640, Seattle, WA 98195-1640.
E-mail: emaroon@uw.edu

DOI: 10.1175/JCLI-D-14-00188.1

the NH, affecting the location of the ITCZ. The atmosphere-only model of Philander et al. (1996) was coupled to both a fixed SST boundary and a fully dynamic ocean, did not include topography, and required stratus-cloud feedbacks to see a large movement of the ITCZ to the NH. Xie (1996) explains how such a WES mechanism can be propagated westward and argues that the structure of the eastern coast is key.

Xu et al. (2004) and Takahashi and Battisti (2007a) have argued that the presence of the Andes in models can be an important asymmetry that keeps the Pacific ITCZ north of the equator in the annual mean. The mountains block midlatitude westerlies, and air is forced to follow isentropic surfaces to the north and south (Terra and Mechoso 2003). Drier air subsides as it moves toward the tropics, where it turns westward, enhances the SH trade winds and dries the SH tropics (Rodwell and Hoskins 2001). Takahashi and Battisti (2007a) tested the influence of the Andes on tropical precipitation relative to the influence of other mountain ranges; they found that the presence of the Andes was more important to the location of the Pacific ITCZ than the Rockies or the Tibetan Plateau. This topographic theory cannot, however, explain the greater NH precipitation in the Atlantic basin, as there is no equivalent to the Andes range in western Africa. They presented simulations that added an Andes mountain range with both a mixed layer ocean (similar simulations as we are about to show results for) and fixed SST and found that coupling the model to a simple mixed layer ocean was essential for increasing tropical precipitation in the NH: changing SSTs through ocean–atmosphere surface flux feedbacks are important for the location of precipitation.

In contrast to these local tropical mechanisms, modeling studies in the past decade have noted a connection between tropical precipitation and extratropical forcing (e.g., Chiang et al. 2003; Chiang and Bitz 2005; Zhang and Delworth 2005; Broccoli et al. 2006; Kang et al. 2008). Paleoclimate data also show evidence of the ITCZ moving during climatic shifts (e.g., Black et al. 1999; Thompson et al. 2000; Koutavas and Lynch-Stieglitz 2003). A study by Fučkar et al. (2013) using an idealized coupled model (Farneti and Vallis 2009) has shown that the location of the zonally averaged ITCZ is determined by the hemisphere with the greater upward heat flux from the extratropical ocean. By opening a channel to create a circumpolar ocean in one hemisphere, deep-water production in that hemisphere is inhibited, pushing the sinking branch of the ocean meridional overturning circulation (MOC) to the opposite hemisphere, which causes the zonally averaged ITCZ to move into the NH.

With greater heat release to the atmosphere in the hemisphere with the sinking branch, an energetic argument proposed by Kang et al. (2009) can be used to explain the tropical precipitation response: greater heat release into the extratropics of one hemisphere means weaker quasi-diffusive energy transport into the extratropics of that hemisphere. Conversely, less heat release from the ocean to atmosphere results in stronger energy transport poleward in that hemisphere. A hemispherically asymmetric poleward transport of energy eventually affects the tropics and the Hadley circulation: a weaker meridional temperature gradient results in a weaker, or summer-like, Hadley circulation in that hemisphere; a stronger gradient strengthens the Hadley circulation. Thus, the zonally averaged ITCZ location, which demarks the equatorward limit of the two Hadley cells, shifts into the hemisphere with deep-water production. As a consequence, there is a net cross-equatorial atmospheric energy transport (AET) into the colder hemisphere (i.e., the hemisphere without deep-water production). Frierson et al. (2013) find observational evidence for this energetic constraint between the tropics and extratropics in satellite and reanalysis data. They point to the Atlantic MOC as the key zonal asymmetry that can explain greater zonally averaged tropical rain in the NH. Kang et al. (2014b) find that the Atlantic MOC is responsible for making the NH warmer than the SH, which also would lead to greater tropical precipitation in the NH.

There are two ways to investigate this asymmetry in tropical precipitation: as a zonal-mean change or as the sum of precipitation changes in individual basins. Both will ultimately yield the same answer but will lead to differing causal interpretations. Here, we favor the zonal-mean approach to examine changes in the closed energy budget. We investigate the roles of local and remote forcing on tropical precipitation in an atmospheric general circulation model. We use the Andes mountain range as our tropical forcing, as well as a variety of surface heat fluxes (also called "q fluxes") to test the relative effectiveness of topography and oceanic heat release in moving tropical precipitation. In section 2, we describe the model we used. Section 3 presents changes in the hydrologic cycle and top-of-atmosphere (TOA) radiation in the simulations that only add an Andes mountain range. Section 4 discusses the results of Andes-only simulations and examines the importance of the WES feedback. The results from simulations with both a mountain range and surface heat fluxes are presented in section 5, and conclusions are presented in section 6.

2. Model description

The model used here is an aquaplanet version of the Geophysical Fluid Dynamics Laboratory Atmospheric Model, version 2.1 (GFDL AM2.1), GCM with a

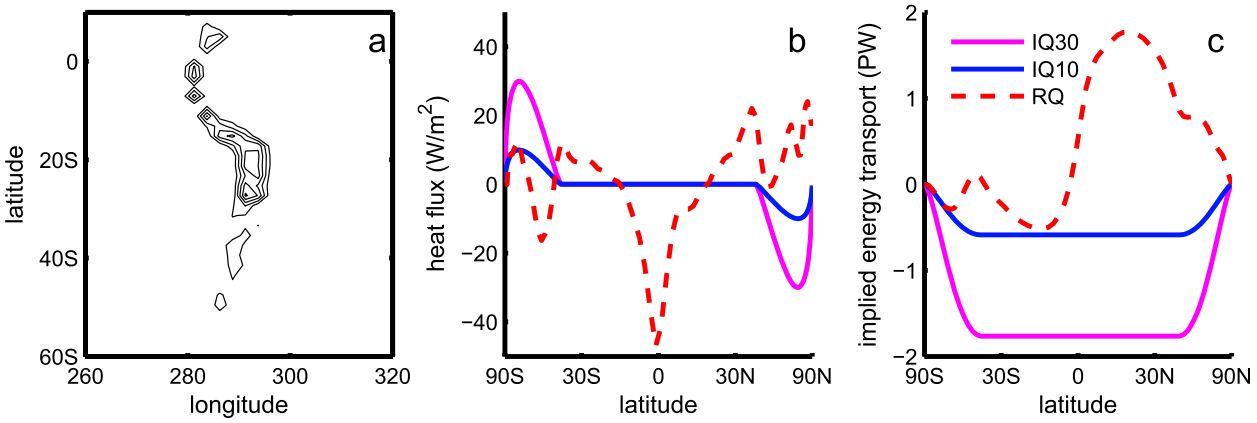

FIG. 1. Topography and surface heat fluxes used in this study. (a) Realistic Andes topography with contours every 1000 m. (b) Zonal q fluxes. Blue and magenta lines show the surface heat flux described in Kang et al. (2008) with peak amplitudes of 10 and 30 W m^{-2} at 65° lat, respectively. The red dashed line is the zonally averaged surface heat flux, as derived from CERES TOA energy and ERA-Interim. (c) The implied northward OET for the surface heat fluxes in (b). Note that the x axes of (b),(c) are area weighted (sine of lat).

finite-volume dynamical core and a slab ocean (Anderson et al. 2004; Delworth et al. 2006). The simulations of Kang et al. (2008) use a similar configuration. An atmospheric GCM coupled to a slab ocean conserves energy (unlike a fixed SST boundary), which allows us to examine the energy budget. All fields that would produce an asymmetric radiative forcing (e.g., ozone) have been symmetrized about the equator. Annual-mean insolation is used. The radiative impact of aerosols is not included. The horizontal resolution is 2.5° × 2°, and there are 24 vertical hybrid pressure–sigma coordinate levels. The heat capacity of the slab ocean is 1×10^7 J K^{-1} m^{-2} (2.4 m). The shallow mixed layer depth decreases integration time and has little effect on the mean climate in comparison to deeper depths (Kang et al. 2008). A relaxed Arakawa–Schubert convection scheme is used for moist convection.

Aquaplanet simulations were completed with realistic Andes topography (T), with zonally symmetric idealized q fluxes (IQ) and real-world q fluxes (RQ), and with combinations of both topography and surface heat fluxes (T + RQ, T + IQ10, and T + IQ30). Figure 1 shows the geometry of the topography and the q fluxes used. All simulations that add topography or q-flux forcing are compared against a flat aquaplanet simulation that does not include q fluxes (the A simulation).

The T simulation uses real-world Andes topography interpolated with a spline fit to the model's grid, and everywhere outside of the Andes topography is flat. The mountains used are "water mountains," where only the height of the surface, not the surface type or roughness, is changed. These simulations have no land. There are also two simulations presented that test the importance of the WES feedback to the response of tropical precipitation. One simulation is flat (NoWES) and one has real-world Andes topography (T + NoWES).

The idealized q flux described in Kang et al. (2008) is used in simulations with amplitudes of 10 and 30 W m^{-2} (IQ10 and IQ30). The real-world zonally averaged q flux is also used: it is derived from the Clouds and the Earth's Radiant Energy System (CERES) TOA energetic budget and the Interim European Centre for Medium-Range Weather Forecasts (ECMWF) Re-Analysis (ERA-Interim; Wielicki et al. 1996; Dee et al. 2011). To insure that the land does not introduce a spurious energy transport into this zonally averaged q flux, the surface flux values over land from these datasets are set to zero, and then this surface flux is zonally averaged and is used for the RQ. The implied ocean energy transport (OET) of these q fluxes indicates that heat is moved southward at all latitudes in IQ10 and IQ30, while in the RQ simulations, the implied heat transport is generally poleward, but is northward at the equator (Fig. 1c). In simulations that have both Andes topography and q fluxes (i.e., T + RQ, T + IQ10, and T + IQ30), the q flux over the water mountains is the same q flux as all other points at that latitude.

Table 1 lists all simulations that will be discussed in the following sections. Simulations were spun up for five years and five additional years beyond the spinup are used for analysis. All results discussed in this paper are robustly defined using these averaging periods.

3. Addition of a single Southern Hemisphere mountain range

a. *Changes in the mean state due to the addition of topography*

In this section, we describe the impact of adding a realistic Andes mountain range to the model. The results

TABLE 1. Description of experiments performed.

Abbreviation	Description
A	Aquaplanet only
T	Realistic Andes topography
NoWES	Flat aquaplanet, no WES feedback
T + NoWES	Realistic Andes topography, no WES feedback
IQ10	Kang et al. (2008) *q* flux, amplitude of 10 W m^{-2}
IQ30	Kang et al. (2008) *q* flux, amplitude of 30 W m^{-2}
RQ	Real-world zonally and annually averaged *q* flux
T + IQ10	Realistic Andes topography and Kang et al. (2008) *q* flux, amplitude of 10 W m^{-2}
T + IQ30	Realistic Andes topography and Kang et al. (2008) *q* flux, amplitude of 30 W m^{-2}
T + RQ	Realistic Andes topography and real zonal *q* flux

using idealized Andes topography are similar to realistic topography experiments (Maroon 2013), so only the latter are described here. Adding a mountain range creates subsidence and equatorward meridional wind to the west of the mountains, as in Takahashi and Battisti (2007a). When westerlies hit the mountain barrier in the subtropics (see Fig. 2a), they are deflected poleward and equatorward, as required by Sverdrup balance (Rodwell and Hoskins 2001). Increased subsidence inhibits precipitation south of the equator, and tropical rainfall is displaced northward on the west side of the Andes (Fig. 3). The decrease of rain in the SH is greater than the increase of rain in the NH; the decrease of SH SST near the Andes is also greater than the very slight increase of NH SST. There is a decrease in the maximum of the zonal-averaged tropical precipitation when adding topography. Evaporation does not change as much as precipitation when adding topography (Fig. 3c).

Increasing SH subtropical subsidence increases the low-cloud amount and decreases high clouds, which both cool the surface (Figs. 2a,b) in the added topography experiment compared to the aquaplanet experiment. Terra and Mechoso (2003) also found an increase in stratocumulus clouds due to the presence of the Andes. As discussed in Takahashi and Battisti (2007a), the addition of Andes topography results in greater subsidence of dry air into the boundary layer, which temporarily increases evaporation and starts cooling. Stratus clouds then act as a feedback to increase the cooling, resulting in a decrease of evaporation once a steady state is reached. The decrease in SST is located in the same region as an increase in low clouds and a decrease in high clouds (Figs. 2a,b). The increase in stratus clouds reduces the insolation reaching the surface, while the decrease in high clouds promotes the escape of radiation to space: this reduces SST and further reinforces subsidence. The changes in

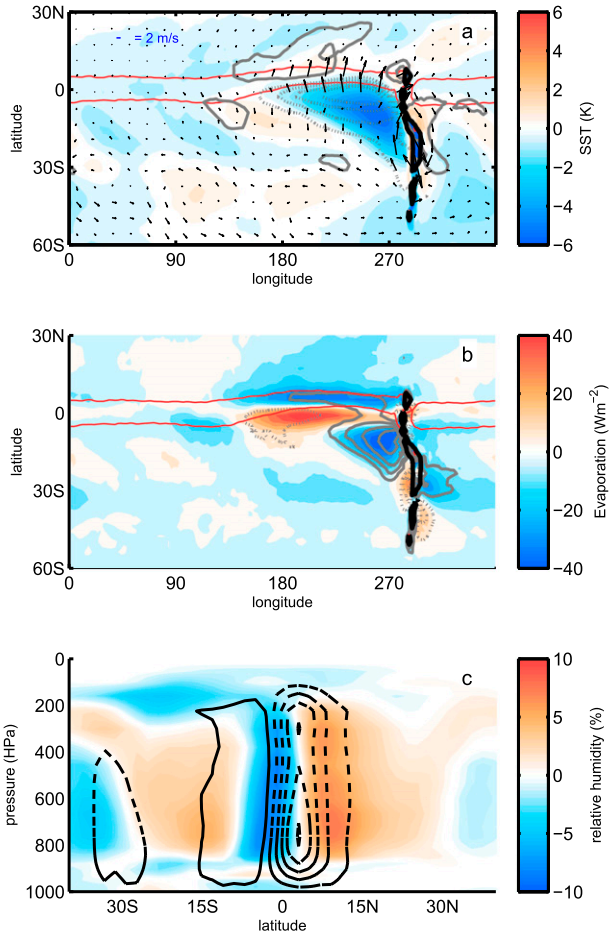

FIG. 2. Changes in streamfunction, SST, clouds, and evaporation. (a) Changes in SST (shading), surface wind (vectors), and high-cloud amount (gray contours) from adding mountains. Vectors represent the change in the winds at the 0.996 (bottom) sigma level. (b) The change in evaporation (shading) and low-cloud amount (contours). The gray solid (dashed) contours in (a),(b) indicate an increase (decrease) in high- and low-cloud amount, respectively; contour intervals are every 10%, and the zero contour is not shown. Black contours indicate topography higher than 1000 m; the red lines show the 10 mm day^{-1} contour of precipitation in the *T* simulation and denote the ITCZ location. (c) The changes of streamfunction (contours) and relative humidity (shading) from adding mountains. Streamlines are displayed every 2×10^{10} kg s^{-1}, starting at 1×10^{10} kg s^{-1}. Solid contours indicate clockwise motion, while dashed contours indicated counterclockwise motion. For comparison, the max Hadley cell streamfunction in the mean climate is approximately 2.5×10^{11} kg s^{-1}.

evaporation are also linked with the changes in low-cloud amount.

The westward extent of the northward precipitation displacement is much greater than the Rossby radius of deformation; this suggests that westward propagation is through some mechanism other than flow deformation due to the topography. Enhanced cross-equatorial winds near the equator would potentially

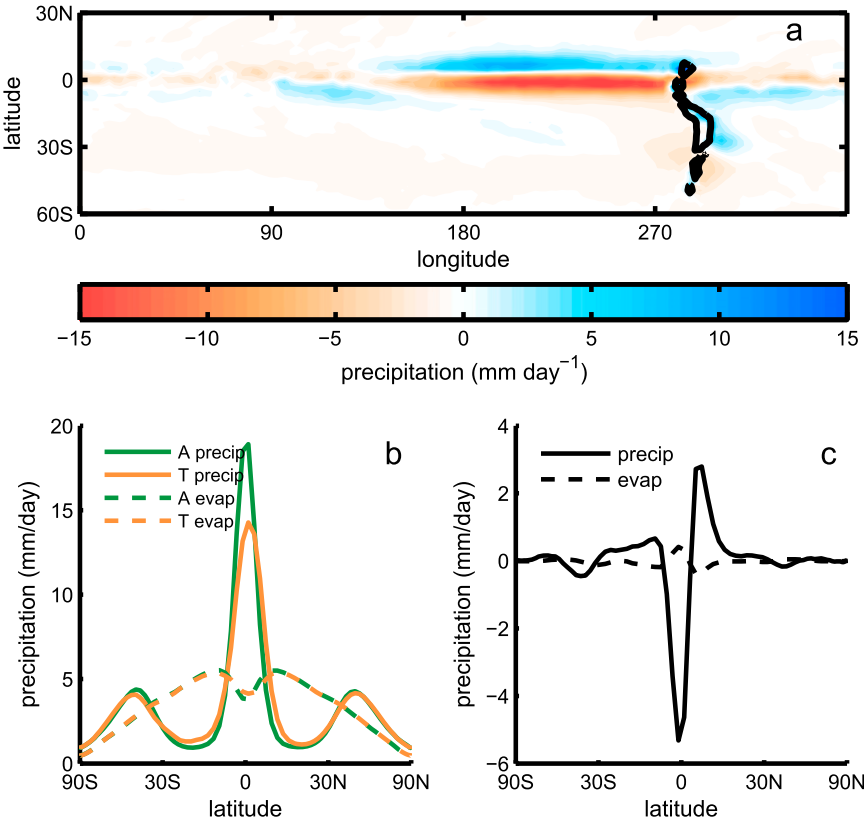

FIG. 3. (a) Change in precipitation from adding topography. Black contours indicate topography higher than 1000 m. (b) Zonally averaged precipitation (solid lines) and evaporation (dashed lines) in the aquaplanet (green lines) and Andes topography (orange lines) simulations. (c) The difference in precipitation and evaporation from adding topography. Note that the x axes of (b),(c) are area weighted (sine of lat).

indicate that a WES feedback is responsible. However, subsidence and associated stratus-cloud feedbacks inhibit convection in the SH, thereby preferring an NH ITCZ with or without a WES feedback. In section 4, we will perform an experiment to examine the importance of the WES feedback for the response of tropical precipitation to topography.

Examining the change in the moisture budget from adding topography shows that the majority of the change in precipitation is balanced by the convergence term (Fig. 3). The change in evaporation opposes the change in precipitation, but it is almost an order of magnitude smaller than the precipitation change. Time- and zonal-mean moisture flux convergence can be further decomposed into the following (see, e.g., Peixoto and Oort 1992):

$$-\nabla\cdot[\overline{v}\overline{q}] = -\nabla\cdot[\overline{v}][\overline{q}] - \nabla\cdot[\overline{v^*}\,\overline{q^*}] - \nabla\cdot[\overline{v'q'}], \qquad (1)$$

where v is meridional velocity, q is specific humidity, and square bracekts indicate the zonal mean.

Terms with asterisks are the anomalies from the zonal mean, and terms with primes are the departure from the time mean. The first term on the right-hand side of Eq. (1) represents the portion of the moisture flux convergence that is attributed to the mean meridional circulation (MMC). The second term is the contribution due to stationary eddies, and the third term is the contribution due to transient circulations. The majority of the change in moisture flux convergence is due to changes in the MMC term (the Hadley circulation) (Fig. 4a). Although one might first think that adding mountains would result in a substantial contribution by stationary eddies this is not the case; the zonal anomalies of specific humidity and meridional wind do not covary. Figure 2a shows that the change in streamlines from the addition of the Andes causes an anomalous cross-equatorial Hadley cell that transports more moisture near the surface into the NH. Moisture has decreased in the SH tropics and subtropics and increased in the midtroposphere of the NH tropics coincident with the anomalous Hadley cell's ascending

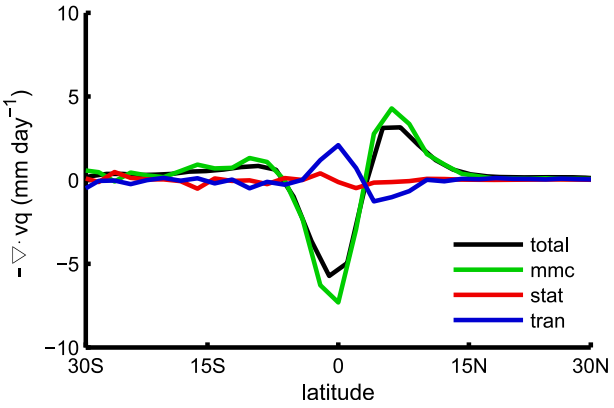

FIG. 4. Decomposition of the moisture flux convergence from adding topography. The total moisture flux convergence (black) is decomposed into the part from the MMC (green), the part from the stationary eddies (red), and the part from the transient circulations (blue).

branch (Fig. 2c). We conducted two additional simulations that doubled and quadrupled the width of an idealized Andes range and found very little change to the magnitude of stationary eddy and MMC terms (not shown). The location of tropical precipitation also did not change from doubling and quadrupling the range's width. Similarly, Takahashi and Battisti (2007b) mention a simulation where they doubled the width of their Andes and found little change in the zonal extent of the Pacific dry zone that they were studying.

b. *Examining the energetic changes in the GFDL AM2.1 simulation with added topography*

Adding topography results in an anomalous transport of energy from the NH to SH (Fig. 5). This southward transport of energy is accomplished by an increase in the transport of energy in the upper branch of an anomalous Hadley cell (recall Fig. 2c) and is consistent with a northward shift in the ITCZ. In the absence of storage by the ocean, the cross-equatorial energy transport can be examined through the TOA radiative imbalance between the two hemispheres:

$$\Delta\mathrm{OET} + \Delta\mathrm{AET} \equiv \Delta\mathrm{TET}, \qquad (2)$$

where

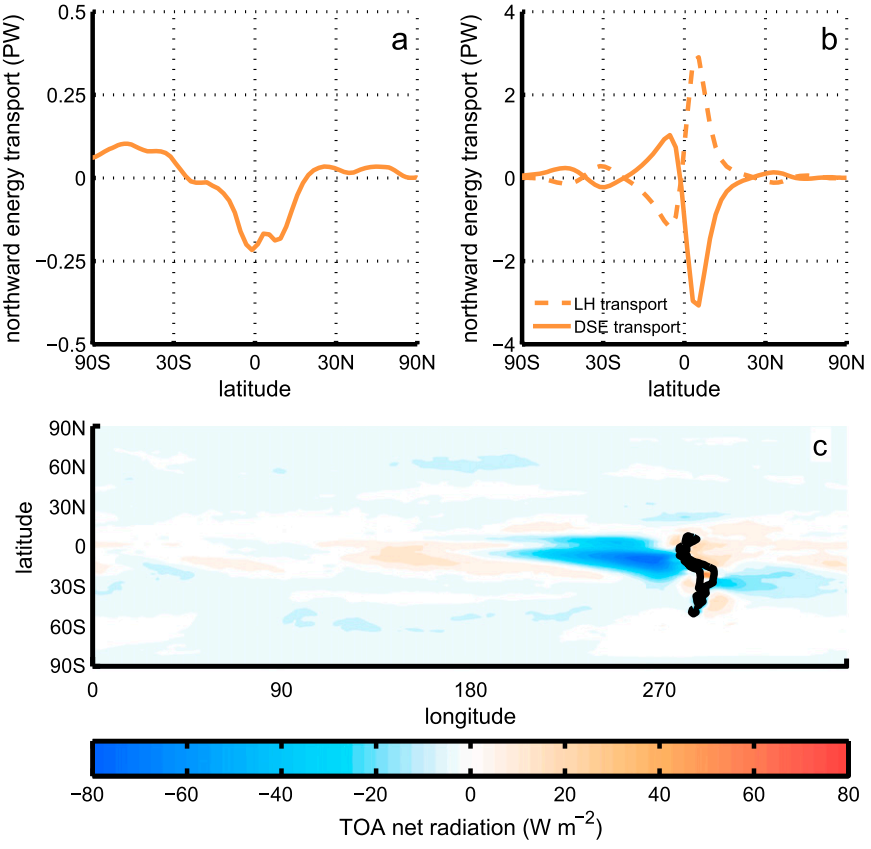

FIG. 5. Change in energy transport from adding topography. (a) Change in total energy transport. (b) Division into latent heat (LH) and dry static energy (DSE) transport. (c) Change in TOA net radiation across the globe (positive downward). The black contour indicates topography.

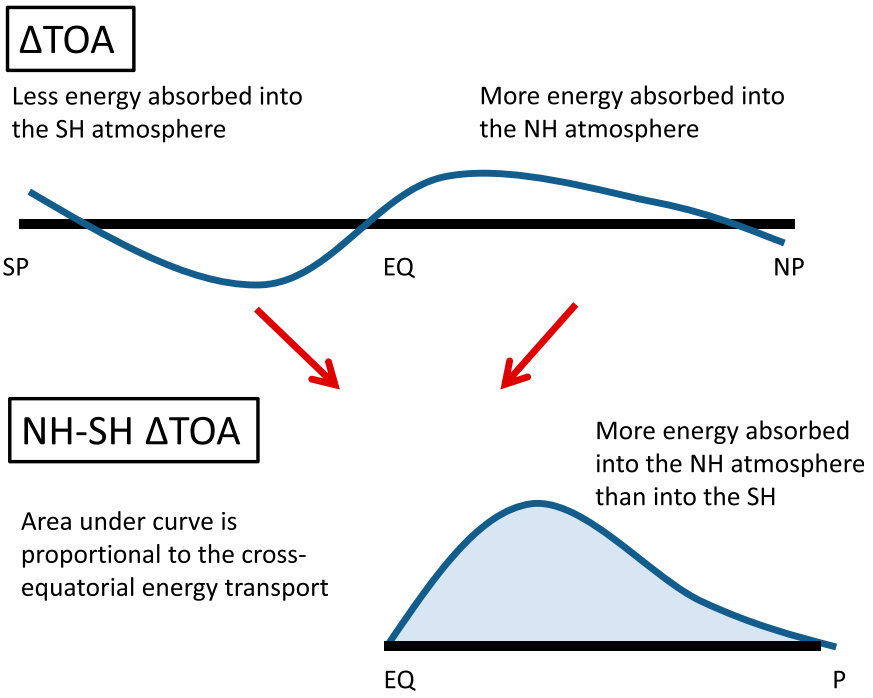

FIG. 6. Schematic showing how changes in TOA absorbed radiation relates to NH − SH changes in radiation and cross-equatorial energy transport.

$$\Delta\mathrm{TET} \equiv \int_0^{2\pi}\int_{-\pi/2}^{0} 2\pi a^2 \cos(\phi)(\Delta\mathrm{SW} - \Delta\mathrm{OLR})\, d\phi\, d\lambda \equiv -\int_0^{2\pi}\int_0^{\pi/2} 2\pi a^2 \cos(\phi)(\Delta\mathrm{SW} - \Delta\mathrm{OLR})\, d\phi\, d\lambda\,, \tag{3}$$

and where ϕ is latitude, λ is longitude, a is the radius of the earth, ΔOET is the change in ocean energy transport at the equator, ΔAET is the change in atmospheric energy transport at the equator, ΔTET is the total meridional energy transport at the equator, ΔSW is the change of net shortwave radiation (with positive defined as into the atmosphere), and ΔOLR is the change in outgoing longwave (LW) radiation (with positive defined as leaving the atmosphere). In the limits of the integral, the equator is 0, and the North and South Poles are $\pi/2$ and $-\pi/2$, respectively. Shortwave and outgoing longwave radiation fluxes are evaluated at model TOA and are integrated over the respective hemispheres.

The change in total meridional energy transport across the equator is exactly balanced by the change in the net energy that enters the climate system (atmosphere and ocean) integrated over either hemisphere. In simulations where OET = 0, all changes in the TOA budget stem from changes in atmospheric energy transport. To illuminate the regions that are important for the change in the energy transport, we rearrange Eqs. (2) and (3) to read as follows:

$$\int_0^{2\pi}\left[\int_0^{\pi/2} 2\pi a^2 \cos(\phi)(\Delta\mathrm{SW} - \Delta\mathrm{OLR})\, d\phi - \int_{-\pi/2}^{0} 2\pi a^2 \cos(\phi)(\Delta\mathrm{SW} - \Delta\mathrm{OLR})\, d\phi\right] d\lambda = -2\Delta\mathrm{TET}. \tag{4}$$

The imbalance in net radiation between the hemispheres is related to the cross-equatorial energy transport. The poleward limit of the integrals is the poles, so Eq. (4) describes the change in the cross-equatorial energy transport in terms of the change in the net hemispheric TOA energy imbalance. The schematic in Fig. 6 translates how a change in the hemispheric imbalance of TOA radiation is related to the cross-equatorial heat transport. A positive change of TOA radiation is defined as an increase in energy absorbed in the atmosphere, and a negative change in TOA radiation is a decrease in absorbed energy (an increase in energy emitted by the atmosphere). The hemispheric imbalance is the NH − SH net (i.e., LW + SW) TOA radiation (NH − SH ΔTOA),

where positive indicates that there is more radiation being absorbed into the NH than into the SH. If the average NH − SH ΔTOA is positive, then more energy has been absorbed in the NH atmosphere than the SH; hence, the change in energy transport across the equator is negative (southward). Conversely, if the average NH − SH ΔTOA is negative, then there is more of an increase in energy absorbed in the SH atmosphere than in the NH, and there is an accompanying northward change in energy transport across the equator.

The average NH − SH ΔTOA is positive because of the addition of Andes topography, indicating that there is greater radiation absorbed in the NH than in the SH. Thus, the change of energy transport across the equator in the atmosphere is southward (Fig. 5). Figure 7 shows how each latitude contributes to the hemispheric average energy imbalance: that is, the change in hemispheric differences in each of the radiative terms [ΔSW(ϕ) − ΔSW($-\phi$), etc.]. Compared to the aquaplanet experiment, in the tropics adding topography causes more OLR to be emitted in the SH than in the NH and more SW to be absorbed in the SH than in the NH. The change in the absorbed SW compensates for most of the change in OLR. The change in the hemispheric imbalance of OLR emitted is greater than the change in the hemispheric imbalance in SW absorbed; that is, the change in the imbalance of OLR contributes slightly more to the anomalous southward heat transport. Within 7° of the equator, the change in SW radiation and OLR is due to the ITCZ shift. The shift of high, thick clouds into the NH leads to a decrease in SW radiation and an increase in OLR within the NH (and vice versa in the SH). The change in the Hadley circulation also decreases the clear-sky OLR in the NH. The sum of these terms leads to a small but positive total NH − SH ΔTOA near the equator (Fig. 7a). NH − SH ΔTOA is largest between 5° and 20° latitude. OLR contributes more to the total ΔTOA on the equatorward side of this region, while SW contributes more on the poleward side.

If the change in TOA net radiation is instead split into clear- and cloudy-sky components, then we see that both net cloudy- and clear-sky radiation contribute to the southward change in the cross-equatorial energy transport, though in different regions (Fig. 7b). At the equator, the cloud-only components of SW and LW (red and green lines, respectively) instead show that the radiative effect of clouds there is to decrease NH − SH ΔTOA in agreement with previous studies (Kang et al. 2008, 2014a; Seo et al. 2014). The positive clear-sky radiation changes are important for maintaining the interhemispheric asymmetry in ΔTOA; decreased humidity in the SH deep tropics occurs where there is anomalous

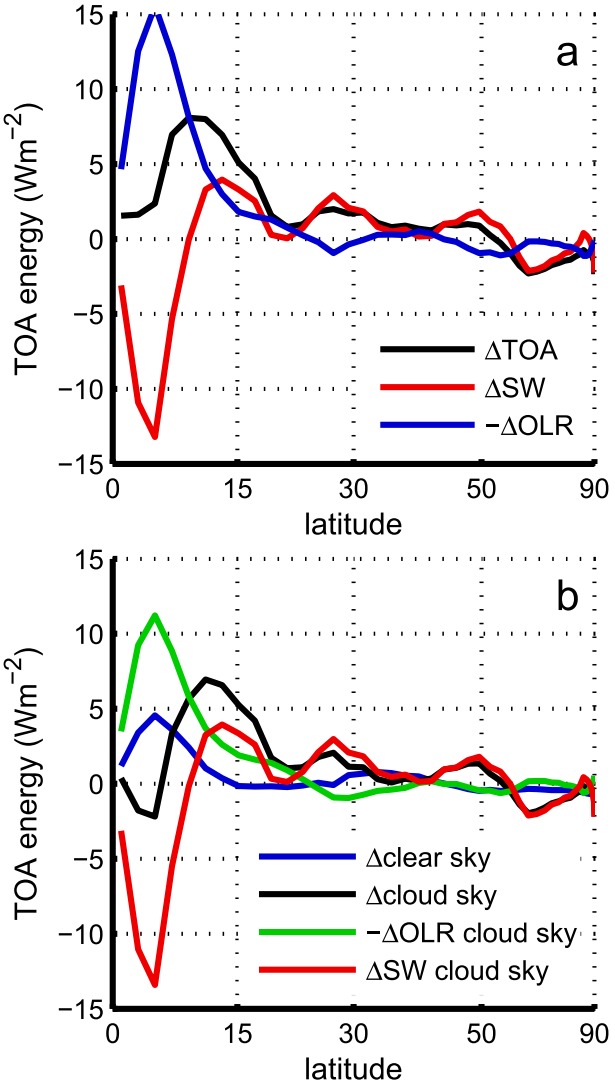

FIG. 7. NH − SH TOA energetic analysis. (a) Change in the TOA radiation asymmetry at each lat from the equator due to the addition of the Andes: net radiation (black), SW (red), and OLR (blue). (b) The decomposition of the change from adding topography of the NH − SH net radiation difference into changes in SW + OLR clear-sky TOA radiation (blue), SW + OLR cloudy-sky radiation (black), OLR cloudy-sky radiation (green), and SW cloudy-sky TOA radiation (red). Positive indicates that there is a greater input of energy at that lat in the NH atmosphere than at the same lat in the SH.

subsidence from the shifted ITCZ. The SW + LW cloud radiation is positive from 5° to 20° (black line) where the contribution from the clear-sky component (blue line) is smaller; at these latitudes in the SH, adding a mountain range has increased the cloud fraction in the low stratus deck, which reduces the absorbed SW insolation. Figure 2a shows that high clouds in the SH (NH) have also decreased (increased), which results in more (less) OLR. This decrease in high cloud is a result of changes in the Hadley circulation at those longitudes. In the NH

(SH), there is less (more) subsidence outside the deep tropics due to the weaker (stronger) overturning caused by pushing the ITCZ off the equator (Lindzen and Hou 1988); high clouds are then either anomalously enhanced or inhibited, depending on the anomalous subsidence. Together, outside the deep tropics, increased SW reflection from SH low clouds along with increased (decreased) SH (NH) OLR from changes in high clouds decrease the energy absorbed in the SH relative to the NH.

An analysis of the changes from adding topography in the MMC, stationary eddy, and transient circulation terms of the moist static energy (MSE) transport can be done, similar to the analysis of moisture flux convergence in the previous section. In calculating the stationary wave component of MSE transport $[\overline{v^*}\,\overline{\mathrm{MSE}^*}]$, however, we find that the major contribution is directly over the range itself. Calculating the stationary wave component without including the region in the immediate vicinity of the mountain range would give a better estimate of the change to the stationary wave energy transport elsewhere, despite removing a region that is essential for the energy budget to remain closed. Calculating $[\overline{v^*}\,\overline{\mathrm{MSE}^*}]$, while ignoring the contribution over the mountain range itself, shows that the contribution to the stationary eddy transport is small in comparison to changes in energy transport by the MMC, similar to the results for moisture flux convergence.

Adding topography decreases the global-mean surface temperature when compared with the equivalent flat run (Table 2; Fig. 2b). This effect occurs even when discounting the small amount of surface that is elevated by the topography. The increase in stratus clouds is one possible explanation, and the decrease in SH high clouds also could be involved. Most of the cooling occurs between 30°S and 0°, and where there is also the largest increase (decrease) in low (high) clouds.

In simulations that add topography on top of a defined q flux, there is also a decrease in the global-mean temperature, with the exception of the T + IQ30 experiment. In these experiments, there is a large surface cooling collocated with an increase in low clouds in SH subtropics to the west of the added topography, but other far-field regions of the globe have also significantly cooled because of the addition of topography.

4. Removal of wind–evaporation feedback in a simulation with an SH mountain range

Hemispheric asymmetry in the boundary conditions can cause one hemisphere to have greater tropical precipitation than the other. In the previous section, this asymmetry is due to the SH mountain range, which generates a regional circulation that extends westward, far beyond the equatorial radius of deformation. Often the WES is cited as the mechanism for the westward extension of a circulation perturbation. Here, we test if a WES feedback is important for the large-scale response in these model simulations by artificially excluding the impact of wind changes on evaporation. We are testing the effects of having a wind feedback in the surface energy budget. If there is no change in the radiative terms, then in a steady state, evaporation need not change either (Xie 1996).

TABLE 2. Global-mean surface temperature (K) for each simulation. Means are expressed as deviations from the aquaplanet simulation for all other simulations. The mean temperatures for 90°–30°S, 30°S–0°, 0°–30°N, and 30°–90°N are also included. The deviation from the mean of each simulation in these bands is from the aquaplanet mean in those same bands. The std dev of the aquaplanet simulation is 0.17 K in the extratropics and 0.14 K in the tropics. The std dev of other simulations are similar; assuming a simulation has the same std dev with the same number of degrees of freedom as the aquaplanet simulation, then changes greater than 0.15 and 0.12 K are significant at the 95% confidence level in the extratropics and tropics, respectively. Changes in the mean temperature from that of the aquaplanet are italicized if significant at the 95% confidence interval. Changes in the mean temperature of a topography simulation from its flat counterpart are boldface if significant at the 95% confidence interval.

Expt	$\overline{T}_{\mathrm{glo}}$	$\overline{T}_{90°-30°S}$	$\overline{T}_{30°S-0°}$	$\overline{T}_{0°-30°N}$	$\overline{T}_{30°-90°N}$
A	291.1	283.5	298.6	298.5	283.6
Deviation from *A*					
T	***−0.2***	−0.1	***−0.6***	***−0.2***	−0.0
NoWES	*+0.2*	+0.0	*+0.2*	*+0.2*	+0.2
T + NoWES	**−0.1**	**−0.1**	***−0.2***	+0.1	**−0.1**
IQ10	*−0.1*	*+2.5*	*+1.0*	*−1.5*	*−2.5*
T + IQ10	***−0.4***	*+2.5*	***+0.6***	*−1.6*	***−3.0***
IQ30	*−4.8*	*+7.5*	*−1.0*	*−9.5*	*−16.4*
T + IQ30	***−4.5***	***+7.7***	***−0.6***	***−8.9***	***−16.2***
RQ	*+3.0*	*+1.4*	*+0.6*	*+3.6*	*+6.4*
T + RQ	***+2.5***	***+1.2***	**+0.0**	***+3.0***	***+6.0***

The expression for evaporation E used in the model is

$$E = C_q|U|(q_{\mathrm{surf}} - q_{\mathrm{atm}}), \tag{5}$$

where C_q is the drag coefficient of moisture determined by Monin–Obukhov drag theory, $|U|$ is the absolute magnitude of the wind in the lowest sigma layer of the atmosphere, q_{surf} is the saturated specific humidity at the surface temperature, and q_{atm} is the specific humidity in the first layer of atmosphere. Variable $|U|$ is calculated using the surface wind magnitude and includes a gustiness parameter to account for unresolved wind speed variability; in all simulations here, this gustiness parameter is zero. In simulations with the WES mechanism removed (the NoWES experiments), $|U|$ is prescribed as a function of latitude in Eq. (5), is taken from the flat aquaplanet simulation, and is symmetrized about the equator. This

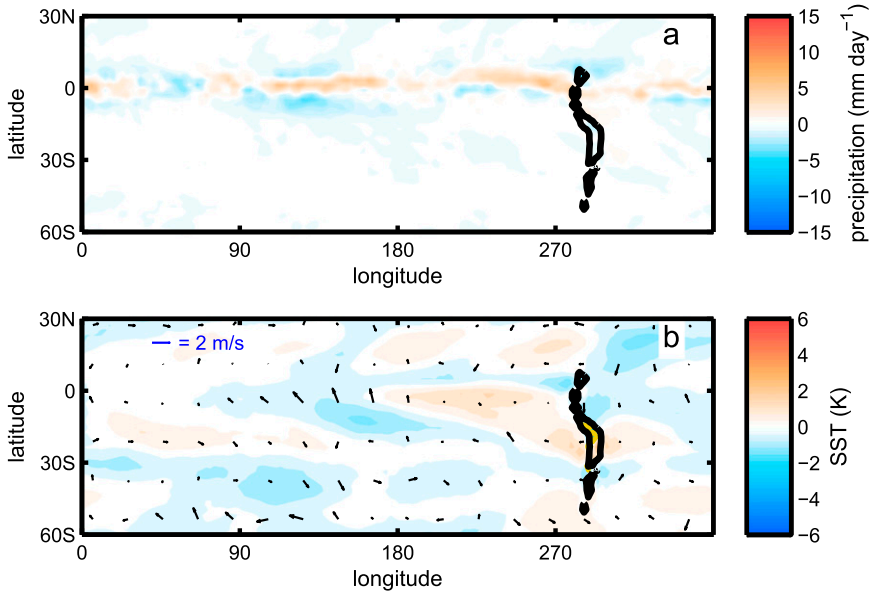

FIG. 8. The impact of WES in setting the response to realistic topography. Shown is the difference of the change from adding topography in a NoWES framework and the change from adding topography in a framework with WES. (a) Precipitation (shading) $[(P_{T+\mathrm{NoWES}} - P_{\mathrm{NoWES}}) - (P_T - P_A)]$. (b) SST (shading) and wind (vectors). Vectors are the winds at the 0.996 sigma level (near surface). Black contours indicate topography higher than 1000 m.

prescribed $|U|$ is not used in the sensible heat or surface momentum flux equations. The response of precipitation to removing the dependence of evaporation on wind is small in a flat aquaplanet. Results comparing the flat NoWES simulations with the aquaplanet simulation with WES are discussed in the appendix.

Adding topography shifts the ITCZ northward with or without the wind–evaporation feedback. The difference between the precipitation change from adding topography in a NoWES framework and the precipitation change from adding topography with WES is shown in Fig. 8a $[(P_{T+\mathrm{NoWES}} - P_{\mathrm{NoWES}}) - (P_T - P_A)]$. This quantity is the difference in the impact of adding mountains because of mountain-induced changes in the WES feedback. If WES is important, the difference will be large; if turning off the wind–evaporation feedback is completely unimportant to the regional precipitation, then the differences in Fig. 8a will be near zero. Figure 8a shows that this difference is small in comparison to the precipitation change from adding topography with the normal evaporation parameterization (cf. Figs. 8a and 3a). In fact, without changes in the WES feedback, the mountains cause the precipitation to shift slightly more into the NH, although the difference is very small.

The change in the SST pattern (Fig. 8b) that is due to WES feedback is also small compared to changes due to the addition of topography (cf. Figs. 8b and 2b). Similarly, the cloud changes due to the orography with WES feedbacks are very similar to the cloud changes without WES feedback. Hence, it is not surprising that the changes in SST due to the presence of mountains is not sensitive to whether or not there are WES feedbacks. With or without WES feedbacks allowed, the addition of mountains shifts the ITCZ northward. Similar results are found in Kang and Held (2012) and Kang et al. (2014a), where the WES feedback is also suppressed in GFDL AM2.1 simulations that look at the impact of various q fluxes; in these studies, both the zonal-mean structure (Kang and Held 2012) and the zonal structure (Kang et al. 2014a) of tropical precipitation are found to be largely independent of the WES feedback. Other studies (e.g., Mahajan et al. 2011; Li and Xie 2014), however, find a large role for the WES feedback. In particular, Mahajan et al. (2011) turn off the WES feedback and find that it is important for amplifying the tropical SST anomaly that results from a high-latitude cooling.

5. The climate response to the addition of both topography and surface heat fluxes

In the experiments described in the previous sections, there were no prescribed q fluxes. In this section, we evaluate the sensitivity of the response to the mountains by modifying the q fluxes to be (i) the zonal average of the real-world q fluxes, found to shift the ITCZ northward in Frierson et al. (2013), and (ii) the idealized midlatitude q fluxes (IQ10 and IQ30) used in Kang et al. (2008, 2009), which shift the ITCZ southward.

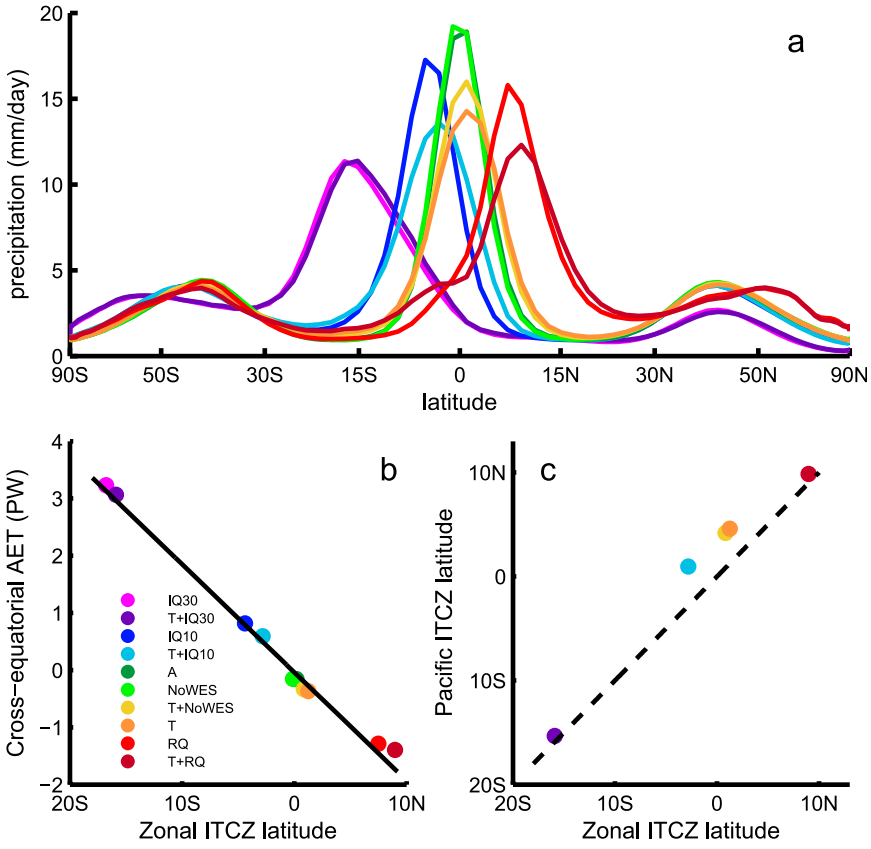

FIG. 9. The range of changes in tropical precipitation. (a) Zonally averaged precipitation in all GFDL AM2.1 experiments. Note that the x axis is area weighted. (b) Lat of the zonally averaged ITCZ vs cross-equatorial AET. The best fit line has a slope of -0.19 PW (° lat)$^{-1}$ ($R^2 = 0.98$). (c) Zonally averaged ITCZ location vs Pacific ITCZ location; the one-to-one line is dashed and denotes if the location of the Pacific ITCZ is identical to the zonally averaged ITCZ; flat simulations are not included in (c).

a. Zonal precipitation response in all simulations

The zonally averaged precipitation for all simulations is presented in Fig. 9a. The ITCZ location is computed by interpolating the zonally averaged precipitation field fit using a cubic spline algorithm and finding the maximum.

The ITCZ location over all q-flux and topography simulations varies greatly, swinging from 16°S to 9°N, depending mainly on the q flux. The response of GFDL AM2.1 is larger than that seen in the real world in the RQ simulation, as evidenced by the greater displacement of the zonally averaged ITCZ in the RQ experiment (8°N) compared to that observed (4°N; Adler et al. 2003). Frierson et al. (2013) argue that this is due to the lack of continents, specifically that of the Sahara Desert, which cools the NH and shifts rainfall southward.

The energetic constraint described in Kang et al. (2009) is valid in these simulations, even when adding a mountain range. In both models, tropical precipitation varies with the magnitude of the energy transport across the equator (accomplished by the Hadley circulation) (Fig. 9b). With a hemispheric imbalance in net absorbed radiation, the Hadley circulation moves energy to the hemisphere with less energy, and the lower branch of the Hadley circulation responds in turn, moving moisture in the opposite direction. The ITCZ in GFDL AM2.1 moves approximately 5° PW^{-1} of cross-equatorial energy transport ($R^2 = 0.98$).

Mountains are expected to affect the zonally averaged precipitation less, since they have a limited regional response, and the results in Fig. 9 confirm this expectation. In general, q fluxes used in this study induce a zonal-mean response of precipitation that is substantially larger than the mountain-induced response. A Pacific ITCZ location is calculated using the zonal average within 120° longitude to the west of the mountain range (Fig. 9c). In the region to the west of the mountain range (where the Pacific Ocean would be), the ITCZ is only slightly farther north than the global-mean ITCZ location of the same simulation.

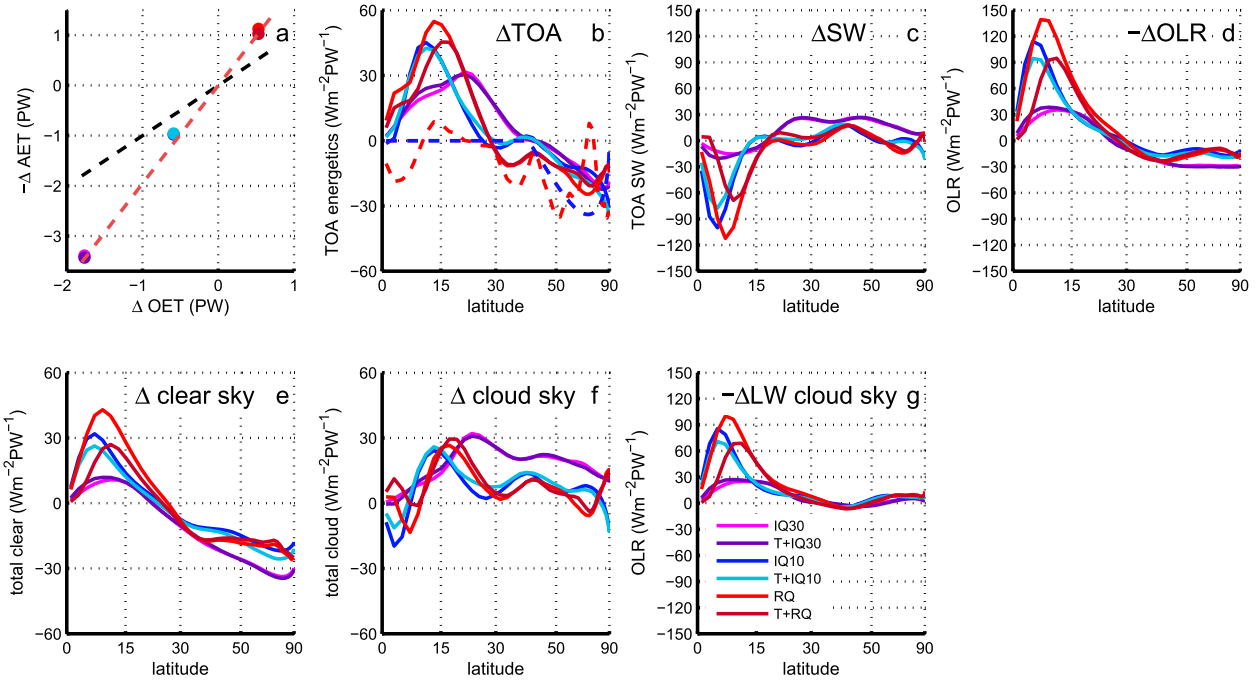

FIG. 10. (a) Compensation of AET to the implied OET at the equator and (b)–(g) the scaled changes in the NH − SH energetics (positive downward). In (a), the black line shows where the simulations of a perfectly compensating model would lie, while the red line with a steeper slope indicates the overcompensation of atmosphere. Colors refer to the same simulations as in Fig. 9. The symbols for the T + IQ30 and IQ30 cases are collocated, as are the T + IQ10/IQ10 and the T + RQ/RQ cases. All values in (b)–(g) have been scaled by the cross-equatorial OET of each simulation. In (b), the change in the hemispheric asymmetry in the net (LW + SW) NH − SH TOA energy is shown as a function of lat for all q-flux simulations. The dashed lines in (b) show the scaled q-flux forcings. If the atmosphere responded completely locally to the forcing, then the TOA energetic term would lie exactly over the dashed line. (c)–(g) As in (b), but for (c) SW TOA (positive indicates into the atmosphere), (d) OLR (positive indicates out of the atmosphere), (e) net TOA clear-sky radiation, (f) net TOA cloudy-sky radiation, and (g) cloudy OLR.

b. *An energetic analysis of the addition of q fluxes in simulations with the same topography*

Here, we define atmospheric compensation as the ratio of cross-equatorial transport of energy by the atmosphere to the cross-equatorial transport of energy by the ocean (into the opposite hemisphere):

$$\frac{\mathrm{AET}_{\mathrm{no\_}Q} - \mathrm{AET}_{Q}}{\mathrm{OET}_{Q} - \mathrm{OET}_{\mathrm{no\_}Q}} = \frac{-\Delta\mathrm{AET}}{\Delta\mathrm{OET}}, \tag{6}$$

where Q denotes an experiment with a q flux and no_Q denotes the corresponding experiment with no added q flux and the same topography as the Q simulation. The symbol Δ then represents the change in the q-flux-added experiment from the otherwise identical experiment without the q flux. The ratio in Eq. (6) is plotted in Fig. 10a for each of the experiments with a q flux. The best fit line for the experiments is in red; overcompensation is indicated by a slope that is steeper than the one-to-one line (black line), while a shallower slope indicates that the atmosphere undercompensates.

Expanding upon this definition of compensation illuminates how radiative feedbacks in these GFDL AM2.1 simulations allow so much overcompensation. Total energy transport at the equator must equal the sum of the atmospheric and oceanic energy transport at the equator [Eq. (2)]. If the atmospheric response perfectly compensates the applied q flux, then $\Delta\mathrm{OET} = -\Delta\mathrm{AET}$ and $\Delta\mathrm{TET} = 0$. If the atmosphere overcompensates (as in GFDL AM2.1), then $\Delta\mathrm{OET} < -\Delta\mathrm{AET}$ and $\Delta\mathrm{TET} > 0$. That is, the atmospheric response moves more heat out of the hemisphere than the ocean imports into that hemisphere; the difference is due to an increase in the net incoming energy from changes in the TOA energy fluxes.

Figure 10b shows the change in the symmetry of the TOA radiation for all simulations that include a q flux. The difference in the integrands of Eq. (4) are shown {e.g., $\Delta[\mathrm{SW}(\phi) - \mathrm{SW}(-\phi)]$}, where Δ now refers to the change in an experiment with a q flux from an otherwise identical experiment without the q flux. The lines in Figs. 10b–g have been scaled by the cross-equatorial OET so that the different q fluxes are compared equally; this scaling also changes the sign of simulations so that they all correspond to a 1 PW energy transport northward across the equator that heats the atmosphere in the

NH and cools in the SH. The dashed curves show a scaled ΔOET for each q flux. If the local atmospheric response to the imposed q flux was a local radiative response, then the change in the TOA energy flux would lay exactly on these dashed lines. If atmospheric energy transport compensated for the ocean energy transport locally, then the change in the TOA energetic terms should be zero everywhere (a purely dynamic response).

The integrals of the curves in Fig. 10b are proportional to the $-\Delta$TET in each experiment. If the integral is negative, then the atmosphere is undercompensating; if positive, the atmosphere is overcompensating. It is notable that the TOA radiation imbalance in the extratropics in isolation would lead toward an undercompensating atmosphere: somewhere between a pure radiative and a pure dynamic response. The atmosphere there responds locally to the surface heating by transporting some heat away and by increasing (decreasing) OLR in the NH (SH).

Overall, however, the change in the NH − SH ΔTOA energy imbalance is positive: more energy is exported from the hemisphere than is imported by the ocean. Water vapor and cloud feedbacks are responsible for the overcompensation. The atmosphere is transporting more energy into the SH than the ocean delivered to the NH, and the tropics and subtropics are the important regions. The surface heatings are scaled here such that the q fluxes add (remove) heat to the NH (SH) atmosphere from the surface. However, a positive change in the NH − SH net TOA radiative imbalance indicates that the atmosphere transports even more energy from the NH into the SH. More (less) clear-sky OLR in the SH (NH) and more (less) LW cloud warming due to changes in the Hadley circulation are part of this energetic response (see Figs. 10c–g). With an even greater energy imbalance between the hemispheres, the atmosphere works even harder to transport heat across the equator; hence, the ITCZ shifts farther into the NH.

Figures 10c and 10d decompose the TOA radiation imbalance into the hemispheric asymmetry in net TOA SW and OLR, respectively; Figs. 10e and 10f show the changes in the hemispheric asymmetry in total TOA radiation (OLR + net TOA SW) in clear and cloudy skies, respectively. Both net clear-sky radiation changes (mostly due to changes in LW water vapor absorption) and LW cloud radiation changes play a role in the overcompensation but in different latitude bands. In the deep tropics, SW cloud forcing works against positive cloudy-sky OLR, and the result is that net cloud forcing works against the atmospheric energy transport's overcompensation; this result is also found in Kang et al. (2008) and Seo et al. (2014). However, clear-sky OLR in the tropics acts to amplify the response, unlike total cloud forcing. The response of net clear-sky TOA radiation peaks closer to the equator, while changes in TOA cloudy-sky radiation peak farther into the subtropics. In the extratropics, a northward ocean heat transport causes an increase in the energy lost to space in clear-sky regions in the NH relative to the SH—a loss that is partially compensated for by a gain in energy in cloudy regions.

The different effects of clear- and cloudy-sky radiation on the change in TET sometimes act together and sometimes against each other. A q flux is added that warms the NH and cools the SH extratropics; this heating is eventually felt in the tropics, and convection shifts into the NH. Changes in circulation increase the humidity in the NH tropics and decreases it in the SH; the increase in the NH increases the amount of energy trapped in the atmosphere there (the SH clear-sky OLR is not as important as the NH clear-sky OLR). Less (more) cloudy-sky OLR is emitted to space in the NH (SH) deep tropics because of greater (fewer) deep clouds. In the region with the ITCZ shift, more cloudy-sky OLR is emitted to space in the SH than in the NH due to lower cloud tops and drier air columns. Here, though, SW cloudy-sky radiation due to reflection more than compensates for the changes in cloudy OLR. In the NH subtropics, increased high clouds reduce cloudy-sky OLR there, while decreased high clouds increase cloudy-sky OLR in the SH subtropics. The warmer atmosphere in the NH subtropics emits less clear-sky OLR because of enhanced water vapor. Changes in stratus decks is minimal in these simulations (in the added Andes simulations, stratus clouds play a larger role). Examining all these changes together in an NH − SH context shows that there is more absorbed radiation in both cloudy- and clear-sky conditions in the NH tropics than in the SH tropics, which acts to increase the southward transport of energy across the equator by the atmosphere. The tropical feedbacks are sufficiently large that the southward atmospheric energy transport is even larger than the northward oceanic transport that instigates the asymmetry in the atmosphere. The larger cross-equatorial AET then leads to a larger ITCZ shift.

In Fig. 10, each simulation has been scaled by the OET forcing, so if the atmosphere responded linearly to the magnitude of the q flux, then all simulations would show the same response. In the extratropics, all simulations do seem to be reacting similarly, even in the RQ simulations (red lines) that have a significantly different meridional q-flux structure. The tropical response is not linear, however. The dark purple and magenta lines indicate simulations with the strongest q flux (IQ30), and yet, when scaled, the peak of the response is less per PW than simulations with smaller q fluxes. The width of the ITCZ becomes broader the farther the ITCZ moves

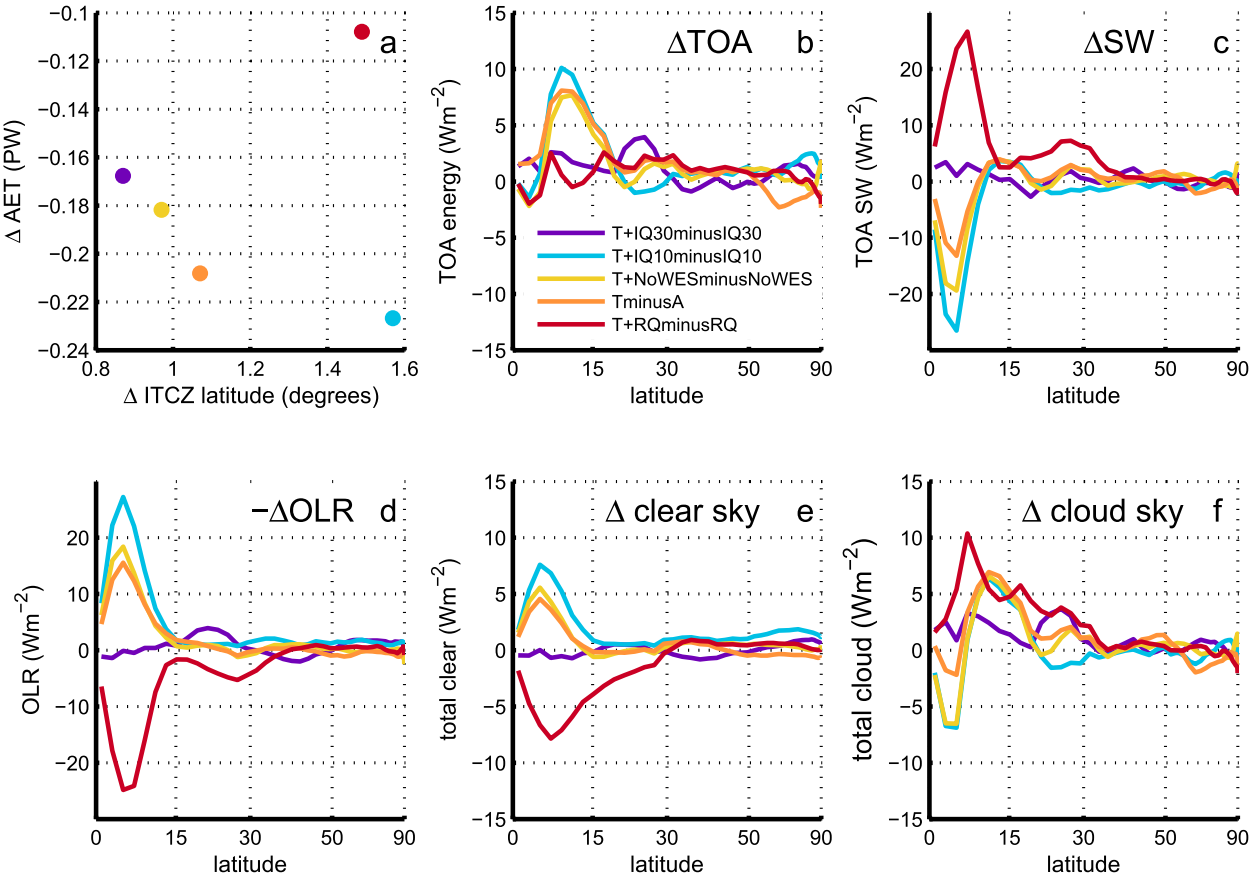

FIG. 11. Change in energy transport and energetic terms in all simulations that include topography. (a) The change in AET vs the change in zonally averaged ITCZ lat in simulations that include topography from their equivalent flat simulations. Differences shown are (T + IQ30) − IQ30 (purple), (T + IQ10) − IQ10 (blue), (T + NoWES) − NoWES (yellow), $T - A$ (orange), and (T + RQ) − RQ (dark red). (b)–(f)The NH − SH changes in TOA radiation budget for these simulations. (b) The change in the hemispheric asymmetry in the TOA radiation balance difference for all simulations that include an SH mountain range. (c)–(f) As in (b), but for (c) absorbed SW (positive downward, energy increases in the atmosphere), (d) OLR (positive upward, energy leaving the atmosphere), (e) TOA clear-sky radiation, and (f) TOA cloudy-sky radiation. Positive indicates that there is a greater change of energy at that lat in the NH atmosphere, while negative indicates that there is greater energy at that lat in the SH.

from the equator, and the differences in the structure and amplitude of the ITCZ shift clearly contribute to the radiative differences in the cases with the largest forcing.

c. *An energetic analysis of the addition of topography in simulations with the same surface heating*

Figure 11a shows the difference in zonally averaged AET of each topography simulation from its flat equivalent versus the difference in the zonally averaged ITCZ latitude. Although all five experiments show a southward AET and a northward-displaced ITCZ, only three of the experiments show the same sensitivity of ITCZ location to energy transport that was found in the q-flux experiments [−0.19 PW (° lat)$^{-1}$]. The other two experiments, and particularly for the case of real heat transport, suggest that the details of the distribution of ocean heat transport affect the atmospheric response to topography. Figures 11b–f show the same quantities as in Fig. 10, but for the impact of adding topography. For example, if the topography simulation also includes a q flux, then its climate response is subtracted with the flat simulation that has the same q flux, leaving only the effect of the added topography. The differences shown in Fig. 11 are (T + IQ30) − IQ30 (purple), (T + IQ10) − IQ10 (blue), (T + NoWES) − NoWES (yellow), $T - A$ (orange), and (T + RQ) − RQ (dark red).

As discussed previously, examining the hemispheric imbalance of TOA radiation illuminates the latitudes that contribute most to the cross-equatorial energy transport; since the latitudinal shift in the ITCZ location due to topography is also proportional to cross-equatorial AET (Fig. 9b), the decomposition of the terms that contribute to the changes in the TOA net

energy flux can be used to interpret the causes of the ITCZ shift. Figure 11 shows this difference for the sets of simulations that add topography while holding q fluxes constant. The TOA imbalance has a similar pattern for those simulations with small q fluxes that do not shift the upwelling branch of Hadley circulation too far from the equator. With the two largest q fluxes (IQ30 and RQ), on the other hand, the TOA patterns induced by topography are significantly different. IQ30 changes the mean climate in such a way that adding topography does not change the climate significantly. With RQ, the ITCZ was already well in the NH before topography was added, so adding topography did not largely change the energy transport by the Hadley circulation across the equator. The changes in SW and OLR compensate from adding topography. A large difference from the addition of topography to the RQ experiment is a larger cold subtropical region to the west of the Andes; here, clear-sky OLR has increased, but cloudy-sky radiation compensates. For the smaller q-flux experiments, the locations of the radiative response to the addition of topography are similar to the same response in sets of simulations that add a q flux and hold topography constant (Fig. 10).

Note that the y axis of Fig. 10 has 4 times the range of those in Figs. 11b–f but that zonal-average TOA changes in Fig. 10 are comparable to some of the regional changes in TOA radiation, as seen in Fig. 5c. Mountains in GFDL AM2.1 cause a strong local TOA response that is less noticeable in a zonal-mean framework. The pattern of tropical clear- and cloudy-sky changes due to the insertion of mountains is similar to those due to q-flux forcing, though weaker in amplitude. Compared to the impact of modest (IQ10) or more realistic amplitude q flux (RQ and IQ30) the impact of topography on the position of the zonal ITCZ or the cross-equatorial energy transport is smaller.

6. Discussion and conclusions

This study has examined the relative importance of cross-equatorial ocean heat flux and Andes-like topography on the location of the zonally averaged atmospheric energy transport and the attendant latitude of the ITCZ. The addition of a q flux with a cross-equatorial ocean energy transport results in large-scale changes to the atmospheric Hadley circulation. Adjustment of the tropical atmosphere responds to amplify the effects of the original q flux; this response produces an overcompensation of the atmosphere in this aquaplanet version of GFDL AM2.1. This response to the q flux occurs regardless of the exact structure of the q flux itself, and with and without the addition of an Andes mountain range. This overcompensation is likely to be robust to the details of ocean circulation.

Adding an Andes-like mountain range results in a small northward shift in tropical precipitation. Although the extent of the displacement is sensitive to the details of the tropical ocean heat transport, in all cases, the changes in the precipitation are related to changes in the location of the ascending branch of the Hadley circulation. The result that tropical precipitation shifts northward is robust with or without wind–evaporation feedback included in the evaporation parameterization. The westward propagation of the northward precipitation displacement is not caused by the WES mechanism in this model.

Adding extra surface heat into one hemisphere shifts precipitation toward that hemisphere. With a mountain range and q flux, the effects on the ITCZ are roughly additive. The addition of a realistic q flux has a greater effect on the location of the ITCZ than does the addition of an Andes-like mountain range. Locally, the changes in the various components of the TOA radiation fluxes (in both cloudy and clear skies) due to an added Andes range are similar to the analogous TOA changes from an added q flux, albeit much smaller in amplitude. In the zonal mean, however, adding a q flux results in a greater shift in tropical precipitation than adding an SH mountain range does. Additional simulations that doubled and quadrupled the width of an idealized Andes did not result in a greater cross-equatorial energy transport or northward displacement of tropical precipitation. The changes in the MMC and stationary eddy components of the moisture and MSE transports also did not change much with increasing width. This result suggests that an Andes range affects the circulation of the tropics most through changing the Hadley circulation, rather than through the creation of stationary eddy circulations (as is seen in the extratropics).

The changes in the stratus-cloud deck with an Andes mountain range reflect insolation and cool the surface, making the SH less conducive for deep convection. In the energetic budget, we find that the increased SW reflection in the SH subtropics is partly responsible for the interhemispheric TOA radiative imbalance, which is in turn linked with the cross-equatorial AET and northward displacement of precipitation. In the simulations that add Andes topography, stratus clouds are created only by changing the pattern of subsidence due to the Andes, and without any representation of cold coastal upwelling or related ocean advection along the shore of South America. This result suggests a more secondary role for ocean advection in maintaining these low clouds. In the coupled ocean–atmosphere version of GFDL AM2.1, this stratus-cloud deck is not well reproduced, and coupled

feedbacks strongly amplify cloud deficiencies that already existed in the atmosphere-only GCM (Wittenberg et al. 2006). More work is necessary to determine the relative importance of ocean dynamics and large-scale subsidence on South Pacific marine stratocumulus.

Changes in the high clouds and moisture due to the shift in the Hadley circulation are important in the simulations that add both topography and q fluxes. The LW cloudy- and clear-sky feedbacks are important components of the interhemispheric energy imbalance and corresponding shift of tropical precipitation. In the simulations with q fluxes, cloud and clear-sky feedbacks are responsible for the overcompensation of the GFDL AM2.1 atmosphere to a given q flux.

Simulations with the same q fluxes and topography described here have also been completed with the GFDL gray-radiation aquaplanet moist model (GRaM) (Frierson et al. 2006). GRaM lacks cloud and clear-sky radiative feedbacks, and given the results here, it is not surprising that the atmosphere undercompensates for a given forcing [see also Seo et al. (2014)]. Aside from the smaller magnitude of climate response, the results were similar to those in the GFDL AM2.1 simulations here. Adding Andes topography shifts precipitation northward, and the precipitation shifts more for a large q flux than for added topography. In these simulations, the dependence of evaporation on wind was also removed, and this removal did not significantly affect the change in precipitation (Maroon 2013). In the GRaM simulation with added Andes, the northward shift of precipitation occurred within about 40° longitude of the Andes (cf. to an extent of about 120° in the GFDL AM2.1 simulations in Fig. 3a); cloud and clear-sky radiative feedbacks, which are present in GFDL AM2.1, may be responsible for the westward extent.

The results from these aquaplanet simulations lend support to recent research showing that the cross-equatorial ocean heat transport is important for the location of the zonally averaged ITCZ and that this result is insensitive to the details of the ocean transport. Using zonally averaged ocean heat flux derived from observations is more than sufficient to put the ITCZ in the correct hemisphere. The addition of an Andes range creates zonal variation in precipitation. The location of the ITCZ is modulated by both local and remote effects, and neither should be neglected when working to understand its dynamics.

Acknowledgments. Yen-Ting Hwang calculated the zonally averaged RQ used in this study. The authors would like to thank Carlos Mechoso, Sarah Kang, and one anonymous reviewer for insightful reviews that improved the manuscript. The authors appreciate helpful discussions with Chris Bretheron, Cecilia Bitz, Yen-Ting Hwang, Jack Scheff, Brian Rose, Kyle Armour, and Aaron Donohoe. E.A.M. has been supported by a National Defense Science and Engineering Graduate Fellowship and the NSF Integrative Graduate Education Research Traineeship (IGERT) Program on Ocean Change. D.M.W.F. was supported by a grant from the NSF (AGS-0846641). D.S.B. was supported by a grant from the Division of Earth Sciences at NSF (Award 1338694).

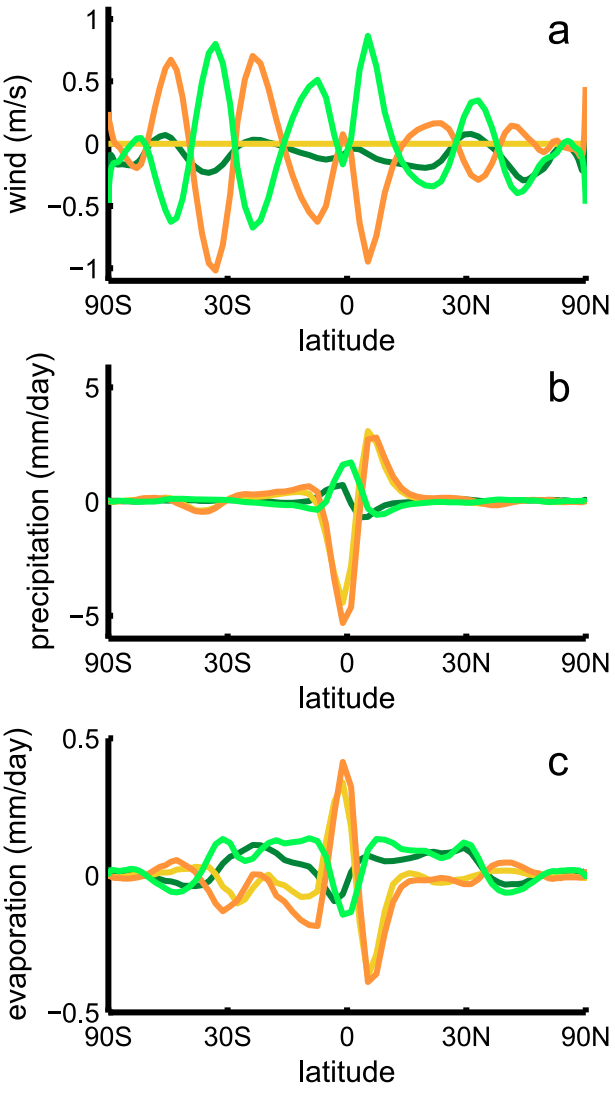

FIG. A1. Zonal-mean changes in wind, precipitation, and evaporation in experiments with and without wind–evaporation feedback. (a) Changes in the wind fed into the evaporation parameterization. (b) Changes in precipitation. (c) Changes in evaporation. Differences of NoWES − A (dark green), (T + NoWES) − T (light green), (T + NoWES) − NoWES (yellow), and T − A (orange) are shown.

APPENDIX

The Response of Removing Wind–Evaporation Feedback in a Flat Aquaplanet

Removing the WES mechanism in an aquaplanet simulation does not change the mean climatology in a significant way (NoWES − *A*). Comparing the flat simulations with and without WES (*A* and NoWES simulations, respectively), there is little change in the zonal-mean wind strength felt by evaporation in each simulation (Fig. A1, dark green line). The wind difference between the simulations with topography and WES (orange) shows that the wind felt by evaporation would otherwise vary much more than it is prescribed. When comparing how evaporation changes in simulations with topography and with or without WES (Figs. A1b–c), we see that adding topography results in a similar change in evaporation from the flat simulation with WES, regardless of whether WES is present or not. The changes in evaporation are almost an order of magnitude smaller than the scale of tropical precipitation changes.

The response of precipitation in a flat aquaplanet to turning off a WES feedback in these simulations is small (Fig. A1b). There is a small southward shift of precipitation when turning off WES [the aquaplanet simulation with WES in GFDL AM2.1 contained a tiny amount of random asymmetry: the ITCZ peaked slightly in the NH tropics (see Fig. 3), and symmetrizing the wind strength in the evaporation parameterization likely helped to symmetrize the climate state].

REFERENCES

Adler, R. F., and Coauthors, 2003: The Version-2 Global Precipitation Climatology Project (GPCP) Monthly Precipitation Analysis (1979–present). *J. Hydrometeor.,* **4,** 1147–1167, doi:10.1175/1525-7541(2003)004<1147:TVGPCP>2.0.CO;2.

Anderson, J. L., and Coauthors, 2004: The new GFDL global atmosphere and land model AM2–LM2: Evaluation with prescribed SST simulations. *J. Climate,* **17,** 4641–4673, doi:10.1175/JCLI-3223.1.

Black, D. E., L. C. Peterson, J. T. Overpeck, A. Kaplan, M. N. Evans, and M. K. Kashgarian, 1999: Eight centuries of North Atlantic ocean atmosphere variability. *Science,* **26,** 1709–1713, doi:10.1126/science.286.5445.1709.

Broccoli, A. J., K. A. Dahl, and R. J. Stouffer, 2006: Response of the ITCZ to Northern Hemisphere cooling. *Geophys. Res. Lett.,* **33,** L01702, doi:10.1029/2005GL024546.

Chiang, J. C. H., and C. M. Bitz, 2005: Influence of high latitude ice cover on the marine Intertropical Convergence Zone. *Climate Dyn.,* **25,** 477–496, doi:10.1007/s00382-005-0040-5.

——, M. Biasutti, and D. S. Battisti, 2003: Sensitivity of the Atlantic Intertropical Convergence Zone to Last Glacial Maximum boundary conditions. *Paleoceanography,* **18,** 1094, doi:10.1029/2003PA000916.

Dee, D. P., and Coauthors, 2011: The ERA-Interim reanalysis: Configuration and performance of the data assimilation system. *Quart. J. Roy. Meteor. Soc.,* **137,** 553–597, doi:10.1002/qj.828.

Delworth, T. L., and Coauthors, 2006: GFDL's CM2 global coupled climate models. Part I: Formulation and simulation characteristics. *J. Climate,* **19,** 643–674, doi:10.1175/JCLI3629.1.

Dima, I. M., and J. M. Wallace, 2003: On the seasonality of the Hadley cell. *J. Atmos. Sci.,* **60,** 1522–1527, doi:10.1175/1520-0469(2003)060<1522:OTSOTH>2.0.CO;2.

Farneti, R., and G. K. Vallis, 2009: An Intermediate Complexity Climate Model (ICCMp1) based on the GFDL flexible modelling system. *Geosci. Model Dev.,* **2,** 73–88, doi:10.5194/gmd-2-73-2009.

Frierson, D. M. W., I. M. Held, and P. Zurita-Gotor, 2006: A gray-radiation aquaplanet moist GCM. Part I: Static stability and eddy scale. *J. Atmos. Sci.,* **63,** 2548–2566, doi:10.1175/JAS3753.1.

——, and Coauthors, 2013: Contribution of ocean overturning circulation to tropical rainfall peak in the Northern Hemisphere. *Nat. Geosci.,* **6,** 940–944, doi:10.1038/ngeo1987.

Fučkar, N. S., S.-P. Xie, R. Farneti, E. A. Maroon, and D. M. W. Frierson, 2013: Influence of the extratropical ocean circulation on the intertropical convergence zone in an idealized coupled general circulation model. *J. Climate,* **26,** 4612–4629, doi:10.1175/JCLI-D-12-00294.1.

Hadley, G., 1735: Concerning the cause of the general trade-winds. *Philos. Trans., Roy. Soc. London,* **39,** 58–62, doi:10.1098/rstl.1735.0014.

Huffman, G. J., and Coauthors, 2007: The TRMM Multisatellite Precipitation Analysis (TMPA): Quasi-global, multiyear, combined-sensor precipitation estimates at fine scales. *J. Hydrometeor.,* **8,** 38–55, doi:10.1175/JHM560.1.

Hwang, Y.-T., and D. M. W. Frierson, 2013: Link between the double-Intertropical Convergence Zone problem and cloud biases over the Southern Ocean. *Proc. Natl. Acad. Sci. USA,* **110,** 4935–4940, doi:10.1073/pnas.1213302110.

Kang, S. M., and I. M. Held, 2012: Tropical precipitation, SSTs and the surface energy budget: A zonally symmetric perspective. *Climate Dyn.,* **38,** 1917–1924, doi:10.1007/s00382-011-1048-7.

——, ——, D. M. W. Frierson, and M. Zhao, 2008: The response of the ITCZ to extratropical thermal forcing: Idealized slab-ocean experiments with a GCM. *J. Climate,* **21,** 3521–3532, doi:10.1175/2007JCLI2146.1.

——, D. M. W. Frierson, and I. M. Held, 2009: The tropical response to extratropical thermal forcing in an idealized GCM: The importance of radiative feedbacks and convective parameterization. *J. Atmos. Sci.,* **66,** 2812–2827, doi:10.1175/2009JAS2924.1.

——, I. M. Held, and S.-P. Xie, 2014a: Contrasting the tropical responses to zonally asymmetric extratropical and tropical thermal forcing. *Climate Dyn.,* **42,** 2033–2043, doi:10.1007/s00382-013-1863-0.

——, R. Seager, D. M. W. Frierson, and X. Liu, 2014b: Croll revisited: Why is the Northern Hemisphere warmer than the Southern Hemisphere? *Climate Dyn.,* doi:10.1007/s00382-014-2147-z, in press.

Koutavas, A., and J. Lynch-Stieglitz, 2003: Glacial–interglacial dynamics of the eastern equatorial Pacific cold tongue-Intertropical Convergence Zone system reconstructed from oxygen isotope records. *Paleoceanography,* **18,** 1089, doi:10.1029/2003PA000894.

Li, G., and S.-P. Xie, 2014: Tropical biases in CMIP5 multimodel ensemble: The excessive equatorial Pacific cold tongue and

double ITCZ problem. *J. Climate,* **27,** 1765–1780, doi:10.1175/JCLI-D-13-00337.1.

Lindzen, R. S., and A. V. Hou, 1988: Hadley circulations for zonally averaged heating centered off the equator. *J. Atmos. Sci.,* **45,** 2416–2427, doi:10.1175/1520-0469(1988)045<2416:HCFZAH>2.0.CO;2.

Mahajan, S., R. Saravanan, and P. Chang, 2011: The role of the wind–evaporation–sea surface temperature (WES) feedback as a thermodynamic pathway for the equatorward propagation of high-latitude sea ice–induced cold anomalies. *J. Climate,* **24,** 1350–1361, doi:10.1175/2010JCLI3455.1.

Maroon, E. A., 2013: The location of tropical precipitation in idealized atmospheric general circulation models forced with Andes topography and surface heat fluxes. M.S. thesis, Dept. of Atmospheric Sciences, University of Washington, 69 pp. [Available online at http://www.atmos.washington.edu/~emaroon/master_emaroon_final.pdf.]

Mechoso, C. R., and Coauthors, 1995: The seasonal cycle over the tropical Pacific in coupled ocean–atmosphere general circulation models. *Mon. Wea. Rev.,* **123,** 2825–2838, doi:10.1175/1520-0493(1995)123<2825:TSCOTT>2.0.CO;2.

Mitchell, T. P., and J. M. Wallace, 1992: The annual cycle in equatorial convection and sea surface temperature. *J. Climate,* **5,** 1140–1156, doi:10.1175/1520-0442(1992)005<1140:TACIEC>2.0.CO;2.

Peixoto, J. P., and A. H. Oort, 1992: *Physics of Climate.* American Institute of Physics, 520 pp.

Philander, S. G. H., D. Gu, G. Lambert, T. Li, D. Halpern, N.-C. Lau, and R. C. Pacanowski, 1996: Why the ITCZ is mostly north of the equator. *J. Climate,* **9,** 2958–2972, doi:10.1175/1520-0442(1996)009<2958:WTIIMN>2.0.CO;2.

Rodwell, M. J., and B. J. Hoskins, 2001: Subtropical anticyclones and summer monsoons. *J. Climate,* **14,** 3192–3211, doi:10.1175/1520-0442(2001)014<3192:SAASM>2.0.CO;2.

Schumacher, C., and R. A. Houze Jr., 2003: The TRMM precipitation radar's view of shallow, isolated rain. *J. Appl. Meteor.,* **42,** 1519–1524, doi:10.1175/1520-0450(2003)042<1519:TTPRVO>2.0.CO;2.

Seo, J., S. M. Kang, and D. M. W. Frierson, 2014: Sensitivity of intertropical convergence zone movement to the latitudinal position of thermal forcing. *J. Climate,* **27,** 3035–3042, doi:10.1175/JCLI-D-13-00691.1.

Takahashi, K., and D. S. Battisti, 2007a: Processes controlling the mean tropical Pacific precipitation pattern. Part I: The Andes and the eastern Pacific ITCZ. *J. Climate,* **20,** 3434–3451, doi:10.1175/JCLI4198.1.

——, and ——, 2007b: Processes controlling the mean tropical Pacific precipitation pattern. Part II: The SPCZ and the southeast Pacific dry zone. *J. Climate,* **20,** 5696–5706, doi:10.1175/2007JCLI1656.1.

Terra, R., and C. R. Mechoso, 2003: Orographic influences on the South American climate. Preprints, *Seventh International Conference on Southern Hemisphere Meteorology and Oceanography,* Wellington, New Zealand, Amer. Meteor. Soc., 100–102.

Thompson, L. G., E. Mosley-Thompson, and K. A. Henderson, 2000: Ice-core palaeoclimate records in tropical South America since the Last Glacial Maximum. *J. Quat. Sci.,* **15,** 377–394, doi:10.1002/1099-1417(200005)15:4<377::AID-JQS542>3.0.CO;2-L.

Waliser, D. E., and C. Gautier, 1993: A satellite-derived climatology of the ITCZ. *J. Climate,* **6,** 2162–2174, doi:10.1175/1520-0442(1993)006<2162:ASDCOT>2.0.CO;2.

Wielicki, B. A., B. R. Barkstrom, E. F. Harrison, R. B. Lee III, G. L. Smith, and J. E. Cooper, 1996: Clouds and the Earth's Radiant Energy System (CERES): An Earth Observing System experiment. *Bull. Amer. Meteor. Soc.,* **77,** 853–868, doi:10.1175/1520-0477(1996)077<0853:CATERE>2.0.CO;2.

Wittenberg, A. T., A. Rosati, N.-C. Lau, and J. J. Ploshay, 2006: GFDL's CM2 global coupled climate models. Part III: Tropical Pacific climate and ENSO. *J. Climate,* **19,** 698–722, doi:10.1175/JCLI3631.1.

Xie, S.-P., 1996: Westward propagation of latitudinal asymmetry in a coupled ocean–atmosphere model. *J. Atmos. Sci.,* **53,** 3236–3250, doi:10.1175/1520-0469(1996)053<3236:WPOLAI>2.0.CO;2.

——, and S. G. H. Philander, 1994: A coupled ocean–atmosphere model of relevance to the ITCZ in the eastern Pacific. *Tellus,* **46A,** 340–350, doi:10.1034/j.1600-0870.1994.t01-1-00001.x.

Xu, H., Y. Wang, and S.-P. Xie, 2004: Effects of the Andes on eastern Pacific climate: A regional atmospheric model study. *J. Climate,* **17,** 589–602, doi:10.1175/1520-0442(2004)017<0589:EOTAOE>2.0.CO;2.

Zhang, C., 2001: Double ITCZs. *J. Geophys. Res.,* **106,** 11 785–11 792, doi:10.1029/2001JD900046.

Zhang, R., and T. L. Delworth, 2005: Simulated tropical response to a substantial weakening of the Atlantic thermohaline circulation. *J. Climate,* **18,** 1853–1860, doi:10.1175/JCLI3460.1.